Compression Buckling Tests of Laminated Graphite-Epoxy Curved Panels

D. J. WILKINS*
General Dynamics, Fort Worth, Texas

Ten different orientation arrangements (in various panel thicknesses) were used in fabricating 72 panels. Eighty-four tests were performed, and the range of R/t studied was 100 to 400. All specimens had a 12-in. outside radius and were 13-in. long by 9-in. wide. The results included development of the moire grid-shadow technique and the Southwell plot method for nondestructive testing as well as observations of the effects of orientation and R/t on the buckling behavior and imperfection sensitivity of such shells. Satisfactory correlation was obtained with a laminated anisotropic curved panel analysis using the Rayleigh-Ritz energy method, which included a crude assumption that the thickness variations in the panels could be used to measure imperfection amplitude.

Introduction

THE objectives of the test program were to provide basic experimental data on the behavior of composite curved panels subjected to compressive buckling and to provide specific design data to verify orientations and thicknesses chosen for a fuselage component. The test variables were lamina orientations and laminate thickness. Other variables important to buckling response, such as length, width, radius, and material type, were held constant.

Test Specimens

All of the composite curved plate specimens were laminated graphite-epoxy, and they all had the same geometric configuration with respect to length, width, and curvature. A sketch of a typical specimen is shown in Fig. 1. The specimens were hand-laid using Morganite II/4617, which has lamina properties of $E_1 = 20 \times 10^6$ psi, $E_2 = 2.1 \times 10^6$ psi, $G_{12} = 0.85 \times 10^6$ psi, $\nu_{12} = 0.21$.

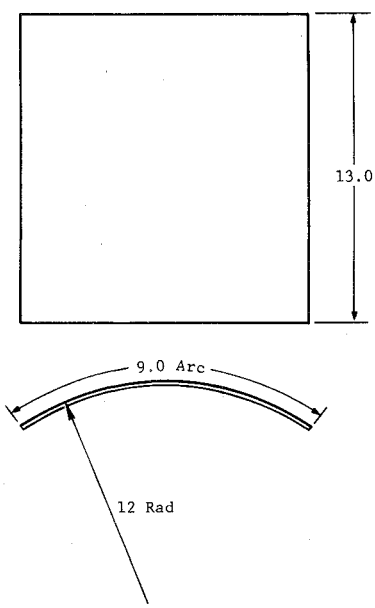

Fig. 1 Curved panel specimen geometry.

Typically, the ultimate strength of this graphite-epoxy material can vary from one material batch to another. However, the stiffness parameters important to stability calculations are quite repeatable. The laminate stiffnesses were calculated by lamination theory using the above lamina properties and were not measured for each individual specimen.

After multiple specimens were laid up on a table, they were draped into a concave steel tool, bagged, and cured. The final operations were to trim the straight edges on a specially jigged table saw and trim the curved edges with an end-mill. No attempt was made to provide "perfect" shells for the tests; therefore, the specimens exhibited the thickness variations common to production parts made with this material. All the specimens had a 12-in. outside radius and were 13-in. long by 9-in. wide before they were installed in the test figure. The inside dimensions after installation in the fixture were 12 in. by 8 in.

Test Procedure Development

The test fixture provided clamped-clamped boundary conditions for the curved edges and either clamped-clamped or simple-simple conditions for the straight edges. Clamping bars provided for variations in thickness of the panels. The test fixture side supports are shown in Figs. 2 and 3.

Variations in the panels' curvature and warpage were slight and were corrected when the panel was installed in the rigid loading fixture. Thus, it was not deemed necessary to measure

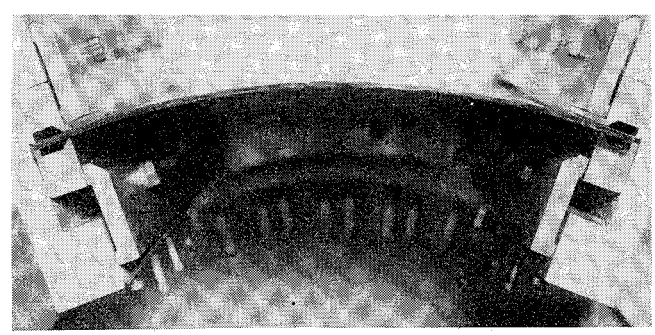

Fig. 2 Top view of test fixure showing simply-supported sides.

Presented as Paper 74-32 at AIAA 12th Aerospace Sciences Meeting, Washington, D.C., January 30–February 1, 1974: submitted February 27, 1974; revision received September 13, 1974. This research was funded by the U.S. Air Force Materials Laboratory, Contract F33615-69-C-1494, with W. R. Johnston, AFML/LC, as Project Engineer. The author gratefully acknowledges the test technique development work of T. S. Love, W. R. Brubaker, and L. J. Herbst.

Index categories: Structural Composite Materials (Including Coatings); Structural Stability Analysis; Aircraft Structural Materials.

* Senior Structures Engineer.

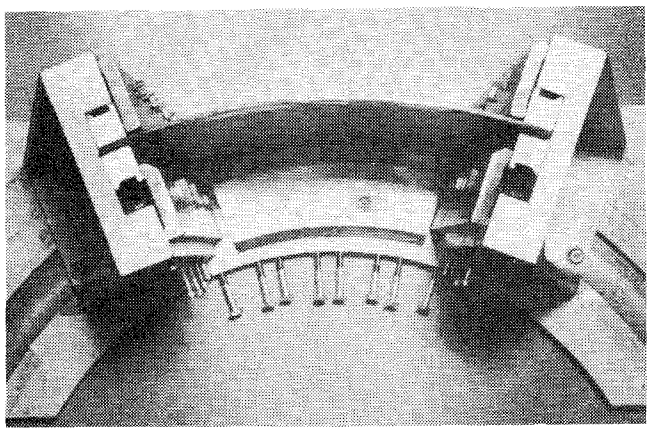

Fig. 3 Top view of test fixure showing clamped sides.

any warpage or curvature variations. Parallelism of loaded edges was determined on installation and corrected, where necessary, before a test run (parallelism to 0.003 in. over the edge length was assumed permissible).

Before each panel was assembled in the test fixture, it was bordered with 0.003-in.-thick Teflon tape at all points that would be contacted by metal. This reduced the shear loads at the edges that resulted from high friction forces.

The structural similarity of the curved panel specimens was such that a reliable test procedure had to be developed and rigidly followed to distinguish clearly between the responses of one panel and another. To aid in this process, the same holding fixture, which accepted various panel thicknesses, was used in all buckling tests. A common procedure for installing the panels and aligning the set-up for test runs proved to be highly relevant in obtaining repeatable and satisfactory results. The salient features in installing the panel were to finger-tighten the bolts on the unloaded edge supports when simple support conditions were used and to wrench-tighten (to 60 in.-lb) the bolts where clamped supports were used. In each case, the bolts were checked after two low-load excursions were applied. These loadings were used to seat the panel and remove most of the hysteresis. After panel installation was completed, an axial load was applied using a 120,000-lb Baldwin Universal test machine.

Curved aluminum panels were also tested to obtain base reference data for evaluating the edge restraints of the fixture. The results from these tests indicated that the clamping action on the loaded edges of the specimens was very near the classical value, however, the simple supports provided slightly more than classical restraint. This excess edge moment was 10 in.-lbs per radian per inch of length. This value was determined to be within acceptable limits and the tests proceeded without further alterations in set-up procedures.

In the buckling test, the information required was out-of-plane movement of the panel as the axial load was increased from 100 lbs to the critical load level. This movement was monitored by two methods: a linear differential transformer whose output was sent to a machine-mounted x-y drum recorder and by the moire shadow method.

When the panels were built, they were intended for one test data point. However, before testing began, the Southwell plot method of nondestructive buckling test was found to be applicable to shell structures. A requirement of the Southwell method was knowledge of where the first buckle would form. This requirement led to further investigation of the moire grid-shadow technique of full-field displacement monitoring. Development work was done on both methods. After this work, the moire technique provided a lower bound buckling criterion, and the Southwell method provided an upper bound buckling criterion. Both methods were subsequently used to provide nondestructive buckling estimates for each panel, although some panels were allowed to snap through.

Moire Grid Shadow Method

The moire grid shadow method is an experimental procedure used to measure out-of-plane movements of a surface. Its principal advantage, especially for buckling tests, is that a full-field view of surface movements can be observed as the test progresses. A brief description of how the method works and the equipment used in its application on the panel studies are explained in the following paragraphs. Development of this procedure was based on the work of Dykes.[1]

The essential pieces of equipment used in developing the moire patterns are a master grid pattern and a rigid transparent backing plate to hold the grid next to the panel. Locations of these elements on a typical test are sketched in Fig. 4. In the experiments described in this paper, a Kodak Carousel projector was used for the light source, and a mounted plexiglass plate, which was formed to the same contour as the specimen, was used to hold the grid pattern in place. With this setup, the grid shadow was obliquely cast on the white-painted surface of the panel. The observer, who looked through the master grid, saw two grids superimposed, and as the panel points moved to or away from the master grid, the shadowed grid would move up or down by the amount

$$y = \delta \tan \alpha$$

When the panel deflected a distance equal to the pitch, P, of the master grid, a dark band or fringe would appear. Therefore, the shape and width of the fringe as well as the number of fringes seen in an area were functions of the change in curvature of the panel over the given area and the grid pitch. For example, a local buckle or a tight hump in the panel would display narrow and closely spaced fringes, whereas an overall buckle would show wide fringes, which would be spaced far apart. On the other hand, if the grid pitch were halved, the sensitivity of the set-up would be doubled, or, twice as many fringes per unit deflection would be seen. The type of grid originally used in the buckling test was determined by assuming a sensitivity of one fringe per 0.01-in. deflection would be desirable. Using the above equation, it was determined that 0.017-in./grid lines, or approximately 50 lines per in., would be acceptable. Buckling tests with this pattern showed promising results, but a need for more sensitivity was required to obtain a better definition of the panel's deflection. Subsequent tests showed that grids with 100 lines/in. gave satisfactory results.

Before a test run, the differential transformer's plunger was lightly spring-loaded against the panel and displaced such that a null balance was achieved at the recorder. The location of the plunger relative to the panel was established by viewing the

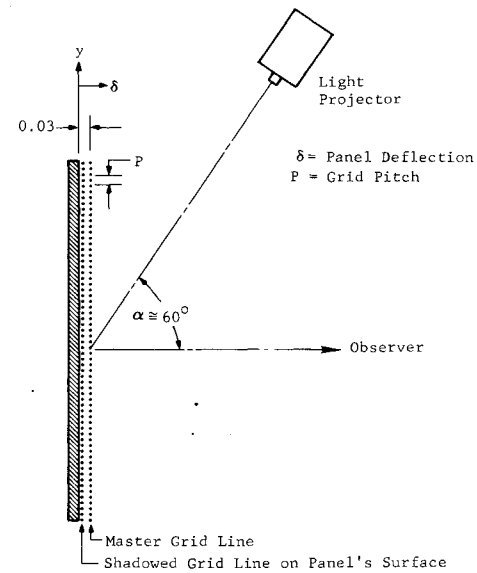

Fig. 4 Test set-up using the moire grid shadow method.

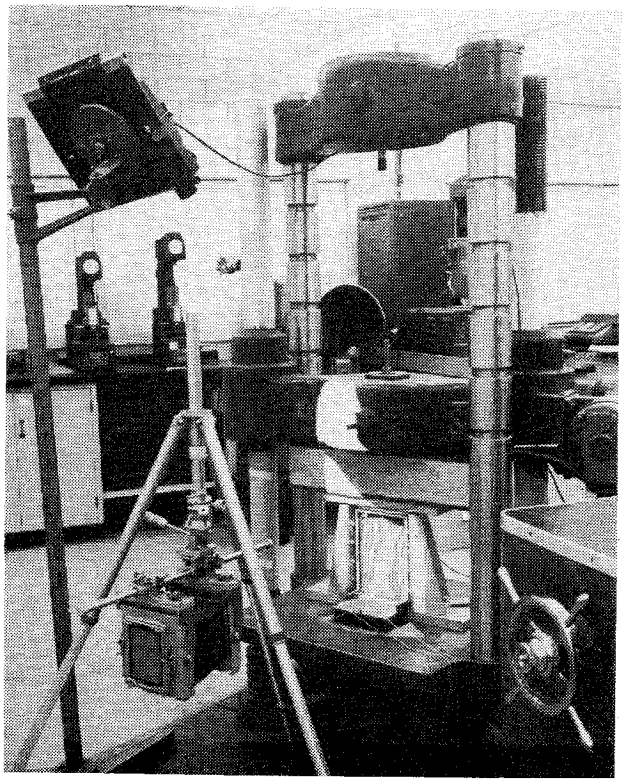

Fig. 5 Test set-up for buckling investigation.

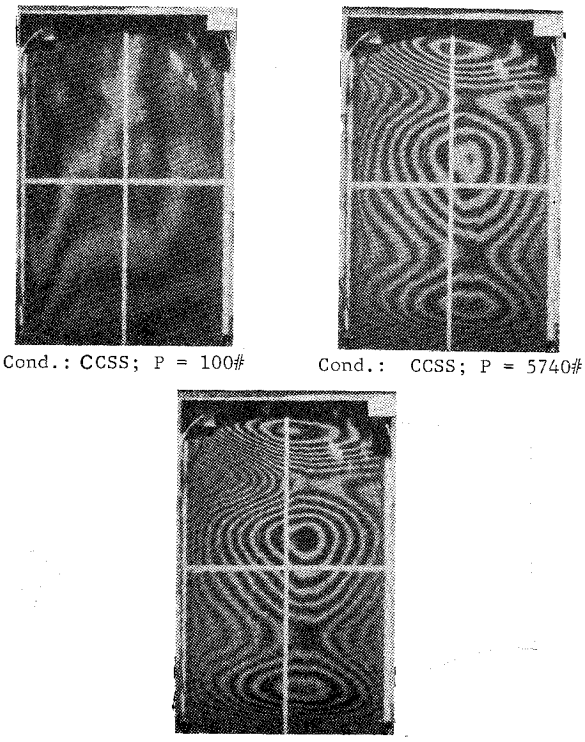

Fig. 7 Moire patterns for −19E.

movements of the moire fringe pattern on the opposite face during the initial loadings. The area with the greatest fringe shift indicated the most out-of-plane activity; thus, the plunger was located at this point to obtain maximum deflections.

The moire patterns, which were developed on the white surface of the painted panel, were used to stop the loading when buckling was observed to be imminent. The characteristics of the pattern at this point were rapid fringe movement and the decreasing distance between adjacent fringes. When these conditions occurred, the load was immediately dumped and the maximum load attained was recorded. The test setup and some representative moire photographs are shown in Figs. 5–8.

Southwell Method

During the time the moire patterns were being observed, a simultaneous plot was made of the out-of-plane motion at an established point on the opposite panel face. This plot of deflection vs load was provided by the test machine's integral recording system. These curves, an example of which is shown in Fig. 9, were used to obtain Southwell plots (see Fig. 10) that ultimately provided the critical buckling load of the panel. The Southwell method is a technique for obtaining the buckling load

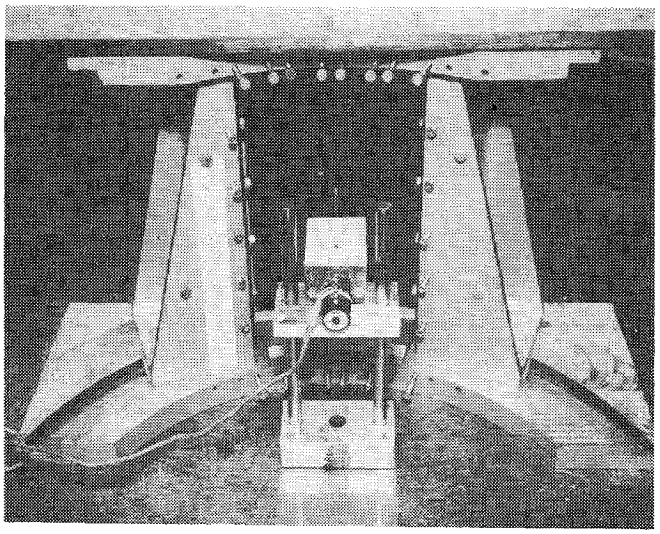

Fig. 6 Rear view of buckling setup.

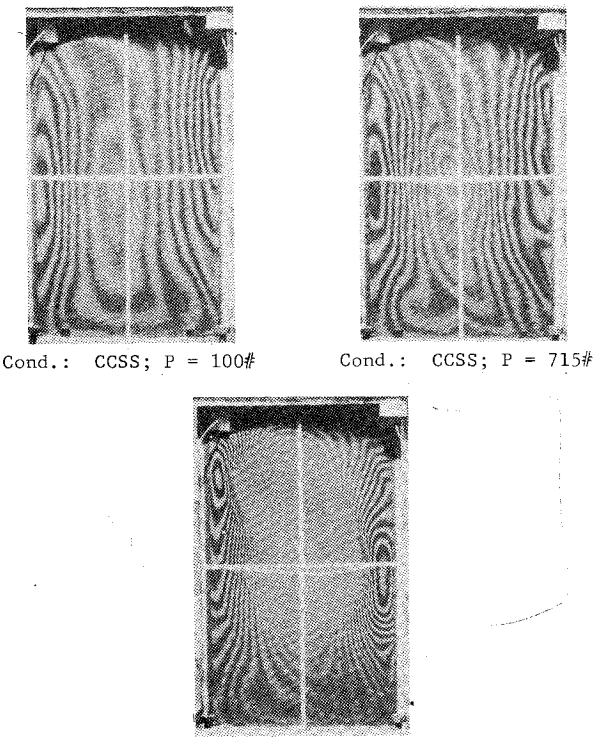

Fig. 8 Moire patterns for −37A.

Table 1 Buckling results for graphite-epoxy curved panels

Panel number	Laminate identification	Mean thickness in.	Thickness mean deviation in.	Vertical edges simply supported, curved edges clamped						All edges clamped		
				Snap load lbs.	Moire load lbs.	Southwell load lbs.	Theor. load lbs.	Knockdown factor Exp.	Knockdown factor Theor.	Snap load lbs.	Moire load lbs.	Southwell load lbs.
17A	$[0/90]_{2s}$	0.0592	0.0021		6680	7323	7200	0.93	0.80		6740	7088
17B	$[0/90]_{2s}$	0.0528	0.0036		4865		5900	0.83	0.73			
19A	$[\pm 45]_{2s}$	0.0696	0.0030		8660	8750	12400	0.70				
19B	$[\pm 45]_{2s}$	0.0707	0.0030	9000		9050	12700	0.71	0.61			
19C	$[\pm 45]_{2s}$	0.0713	0.0025		8820		13000	0.68	0.62			
19D	$[\pm 45]_{2s}$	0.0719	0.0019		8760		13200	0.66	0.59			
19E	$[\pm 45]_{2s}$	0.0598	0.0026		5740		9500	0.60	0.44		5980	
21A	$[0/90]_{s}$	0.0289	0.0015		985	1125	1530	0.64	0.84	1195	1175	
21B	$[0/90]_{s}$	0.0282	0.0013		925		1470	0.63	0.83			
23A	$[\pm 45]_{s}$	0.0354	0.0025	1870	1870	1914	4000	0.47				
23B	$[\pm 45]_{s}$	0.0362	0.0033	1610		1695	4180	0.38	0.35			
23C	$[\pm 45]_{s}$	0.0340	0.0018		1590	1624	3780	0.42	0.35		1625	
23D	$[\pm 45]_{s}$	0.0359	0.0025	1850			4130	0.45	0.47			
23E	$[\pm 45]_{s}$	0.0307	0.0013		1280	1314	2950	0.43	0.46			
29C	$[\pm 45]_{3s}$	0.1045	0.0027		17760	23125	27700	0.64	0.63			
29D	$[\pm 45]_{3s}$	0.1066	0.0037			21889	29200	0.62	0.62			
29E	$[\pm 45]_{3s}$	0.0892	0.0040		10780		19700	0.55	0.52			
31A	$[-45]_{2s}$	0.0343	0.0024	1550	1550	1759	2800	0.55	0.16			
31B	$[-45]_{2s}$	0.0356	0.0038		1505	1704	2900	0.52			1480	
31C	$[-45]_{2s}$	0.0353	0.0017		1520		2900	0.52				
31D	$[-45]_{2s}$	0.0347	0.0021	1500			2800	0.54				
31E	$[-45]_{2s}$	0.0289	0.0015	975			2000	0.49	0.33			
33A	$[-45]_{4s}$	0.0692	0.0031	7050			11700	0.60				
33B	$[-45]_{4s}$	0.0679	0.0024	6340	6300	7000	11300	0.56	0.50			
33C	$[-45]_{4s}$	0.0622	0.0030		5700	5750	9300	0.61	0.24			
33D	$[-45]_{4s}$	0.0709	0.0035		6620		12200	0.54	0.29			
33E	$[-45]_{4s}$	0.0591	0.0024	4000	4000	4021	8300	0.47				
35A	$[-45]_{6s}$	0.0902	0.0049		9180	10270	20000	0.46	0.36			
37A	$[+30]_{2s}$	0.0282	0.0071	725	715		2200	0.33	0.41			
39A	$[+30]_{4s}$	0.0580	0.0022		4730		8000	0.59	0.73		4985	
41A	$[+30]_{6s}$	0.0900	0.0018		10460	10435	17800	0.59	0.84			
43A	$[0]_{2s}$	0.0364	0.0020		1315	1575	2100	0.63	0.68			
43C	$[0]_{2s}$	0.0368	0.0032	1540			2100	0.73	0.64			
43D	$[0]_{2s}$	0.0362	0.0024	1315	1290	1418	2100	0.63	0.64			
43E	$[0]_{2s}$	0.0294	0.0020	945			1800	0.53	0.49			
45A	$[0]_{4s}$	0.0701	0.0018		5580	6468	8700	0.64	0.67		7300	7704
45B	$[0]_{4s}$	0.0699	0.0028	5735			8700	0.66	0.62			
45C	$[0]_{4s}$	0.0696	0.0014		5300	5553	8700	0.56	0.66			
45D	$[0]_{4s}$	0.0695	0.0014		5080	5610	8700	0.58	0.66		6600	7123
45E	$[0]_{4s}$	0.0582	0.0029		5105	5122	5800	0.88	0.64			
47A	$[0]_{6s}$	0.1064	0.0030		16500	18362	21600	0.76	0.61			
47B	$[0]_{6s}$	0.1039	0.0027		18000	19598	20600	0.85	0.62		20560	21538
47C	$[0]_{6s}$	0.1013	0.0035		16760	17812	19600	0.56	0.59			
49A	$[0/90]_{3s}$	0.0880	0.0026		14680	16625	16200	0.91	0.79			
49B	$[0/90]_{3s}$	0.0781	0.0034		12460	14118	12500	0.99	0.79			
51A	$[\pm 30]_{s}$	0.0296	0.0019		1150		2630	0.44	0.55			
53A	$[\pm 30]_{2s}$	0.0557	0.0023		5405	5818	7750	0.70	0.70			
55A	$[\pm 30]_{3s}$	0.0807	0.0026		12900	13860	7000	0.76	0.68			
57A	$[0/45/90/-45]_{s}$	0.0574	0.0018		8240	8966	10000	0.82	0.90			
57B	$[0/45/90/-45]_{s}$	0.0499	0.0028		6640	6691	7500	0.86	0.80			
57C	$[0/45/90/-45]_{s}$	0.0516	0.0023		6460	6897	7900	0.82	0.85		7100	
57D	$[0/45/90/-45]_{s}$	0.0499	0.0028		5820	6416	7500	0.78	0.80			
57E	$[0/45/90/-45]_{s}$	0.0524	0.0032		6960	7194	8250	0.84	0.78			
59A	$[0/\pm 60]_{s}$	0.0422	0.0010		3355	3595	5200	0.64	0.92		3730	3846
59B	$[0/\pm 60]_{s}$	0.0392	0.0018		3390	3626	4450	0.76	0.84	3685	3530	
59C	$[0/\pm 60]_{s}$	0.0382	0.0026		3400	3582	4200	0.81	0.79			
59D	$[0/\pm 60]_{s}$	0.0397	0.0020		3000	3170	4600	0.65	0.82			
59E	$[0/\pm 60]_{s}$	0.0390	0.0028		3460	3846	4420	0.78	0.76			
61A	$[0/\pm 60]_{2s}$	0.0870	0.0026		22950	23871	27400	0.84	0.76			
61B	$[0/\pm 60]_{2s}$	0.0794	0.0041		18080	18571	22800	0.79	0.70			
61C	$[0/\pm 60]_{2s}$	0.0785	0.0034		16920	18136	22300	0.76	0.71			
61D	$[0/\pm 60]_{2s}$	0.0782	0.0029		18800	19000	22300	0.84	0.74			
69A	$[0/\pm 45/0]_{s}$	0.0512	0.0026		5500	5663	8150	0.68	0.63			
69B	$[0/\pm 45/0]_{s}$	0.0521	0.0019	5410	5410	5114	8150	0.62	0.70			
69C	$[0/\pm 45/0]_{s}$	0.0488	0.0028		5385	5604	7400	0.73	0.61			
69D	$[0/\pm 45/0]_{s}$	0.0504	0.0025		5310	5581	7900	0.67	0.63			
69E	$[0/\pm 45/0]_{s}$	0.0506	0.0034	5870	5700	5882	8000	0.73	0.58			
71A	$[0/\pm 45]_{s}$	0.0408	0.0021		2930	3187	4870	0.60	0.75			
71B	$[0/\pm 45]_{s}$	0.0394	0.0019		2595	2803	4540	0.57	0.76			
71C	$[0/\pm 45]_{s}$	0.0394	0.0021	2810	2810	2910	4540	0.62	0.75			
71D	$[0/\pm 45]_{s}$	0.0397	0.0020		2610	2942	4600	0.57	0.75			
71E	$[0/\pm 45]_{s}$	0.0390	0.0025		2310	3333	4440	0.70	0.71			

of a structure from experimental load-deflection information. The details of its implementation differ depending on the structure being analyzed. It has been used for the buckling of columns, beam-columns, plates, and, more recently, shells.

The theoretical basis for the use of the Southwell method for shells may be found in the works of Tenerelli and Horton[2] and Galletly and Reynolds.[3] A modification of the method of Tenerelli and Horton was used here.

Briefly, the moire grid-shadow method was used in the initial load cycle (below the buckling load) to find the point of maximum deflection on the shell. The linear variable differential transformer (LVDT) was then positioned to read deflections at that point. On subsequent load cycles, the load-deflection plot for that point was read out on the rotating drum of the test machine.

The actual Southwell plots were generated by using a Hewlett-Packard 9100B calculator with a plotter. A program was written to take the load-deflection data as input and produce a plot of (deflection/applied load) vs deflection. The straight portion of this plot was used to calculate the buckling load as the inverse of the slope of the line.

The moire procedure used in obtaining buckling loads of the various panels proved to be satisfactory and saved the majority of panels for future tests. However, a number of panels snapped into a post-yield buckle before loading could be stopped. When this occurred, the panels were damaged to the extent that subsequent load cycles produced lower buckling loads. On the other hand, when the loads were dumped at initial evidence of buckling, subsequent loading cycles produced repeatable results. On a few panels, all three methods (moire, Southwell, and snap-through) were used to obtain the critical buckling load. Comparing the results of these methods, using Table 1, it can be seen that satisfactory correlation exists.

Test Results

Only the unidirectional panels tended to break apart after snapping through, and only a few of them actually broke. In a limited study, the multidirectional laminates were shown to retain a high percentage of their buckling strength after repeated buckling. The panels tended to reach a minimum strength after several buckling excursions.

Due to the success of the moire grid shadow method, 14 panels were tested with clamped sides after all panels were first tested with simply supported sides. The test results are presented in

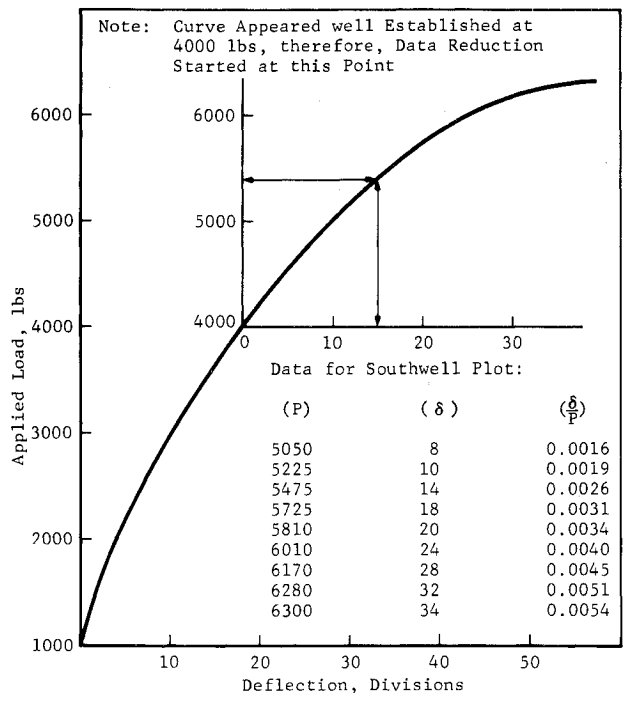

Fig. 9 Typical load-deflection curve

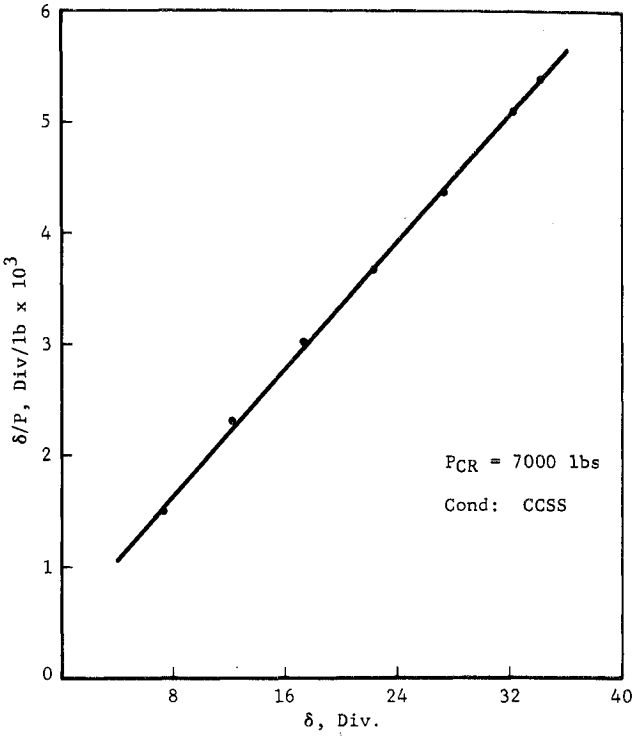

Fig. 10 Southwell curve for −33B.

Table 1. The mean and standard deviation of the thickness of each panel were determined from 25 measurements taken on a 5-by-5 grid. The notation "Thickness Mean Deviation" given in Table 1 is the standard deviation of the thickness from the mean.

Correlation of test result to theory was attempted only for the panels with simply supported sides. The theoretical load given in Table 1 is the classical buckling load as determined by the analysis described below. Two values of the knockdown factor are given in the table. The experimental knockdown factor is the ratio of the snap-through load (or the moire load if no snap-through occurred) to the classical buckling load. The theoretical knockdown factor is calculated from an imperfection sensitivity analysis.

The classical buckling loads were calculated using a Rayleigh-Ritz energy method, whose development has only been published as a limited-distribution company report.[4] The laminated anisotropic behavior and curvature of the panels were recognized in the analysis.

The imperfection sensitivity analysis is based on a modification of the work of Tennyson and his colleagues.[5,6] The referenced

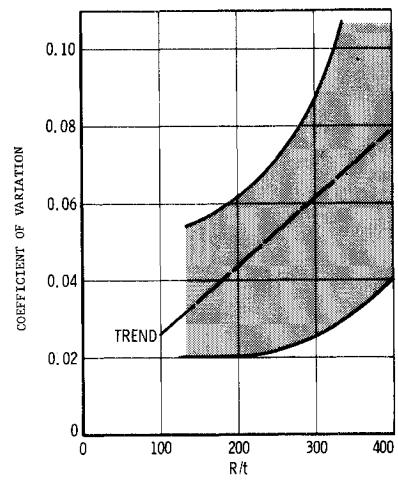

Fig. 11 Thickness coefficient of variation as a function of R/t

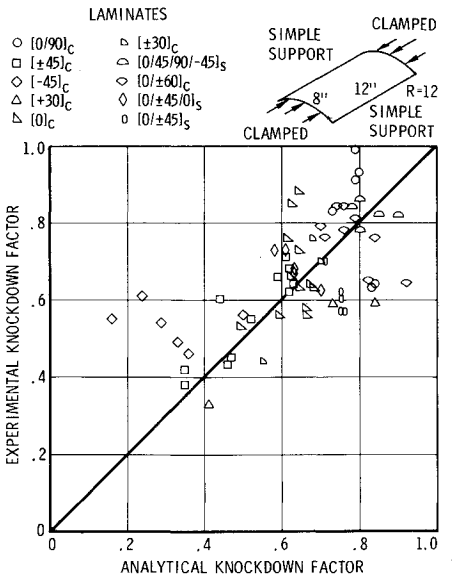

Fig. 12 Correlation of experimental and analytical knockdown factors.

analysis addressed a simply supported full cylinder with a precise axisymmetric shape imperfection. For this study, the standard deviation of the thickness over the shell was used as a measure of imperfection, and the knockdown factor for the full cylinder was assumed to apply to any partial cylinder regardless of boundary conditions. This imperfection assumption is very crude analytically. It was tried because of its simplicity since the approach used in the referenced analysis (Fourier analysis of measured shape) was considered impractical except for laboratory-type testing. The knockdown factor based on standard deviations of the panel thickness is not always conservative, but it does indicate trends fairly well.

A not-too-surprising result from Table 1 is shown in Fig. 11. The range and trend of the coefficient of variation in thickness depend strongly on the absolute thickness and are plotted as functions of R/t to indicate that the decrease in buckling strength with increasing R/t is due partially to the increasing thickness variation.

The applicability of the thickness-based imperfection sensitivity analysis is shown in Fig. 12, where the experimental knockdown factor is plotted against the analytical knockdown factor on the familiar plot where the analyst hopes all data will fall on a 45° line. The correlation obtained indicates that the assumption of the thickness coefficient of variation as the measure of imperfection may not be rigorous enough.

Conclusions

This test program represents the most comprehensive set of experiments performed to study the effects of orientation and R/t on the buckling behavior of laminated composite curved panels. Several interesting conclusions were found. Composite shells suffer from imperfection sensitivity as do metal shells. Composite shells (except those composed of unidirectional laminates) can snap through and return to their original shape when the buckling load is removed; however, their buckling resistance is degraded somewhat. Further, the development of nondestructive test methods for this program could be important for testing questionable production parts whose subsequent performance may be critical to the life of a structure. Finally, the results serve as an experimental data base with which to compare analytical prediction methods for laminated curved panels.

References

[1] Dykes, B. C., "Analysis of Displacements in Large Plates by the Moire Grid-Shadow Technique," *Experimental Stress Analysis and its Influence on Design Conference* (Cambridge, England, April 1970), *Proceedings of the Institution of Mechanical Engineers,* Publishers, London, 1970.

[2] Tenerelli, D. J. and Horton, W. H., "An Experimental Study of the Local Buckling of Ring-Stiffened Cylinders Subject to Axial Compression," *Israel Journal of Technology,* Vol. 7, No. 1–2, 1969, pp. 181–194.

[3] Galletly, G. D. and Reynolds, T. E., "A Simple Extension of Southwell's Method for Determining the Elastic General Instability Pressure," *Proceedings of the Society for Experimental Stress Analysis,* Vol. 13, No. 2, pp. 141–152.

[4] Wilkins, D. J., *Anisotropic Curved Panel Analysis,* Rept. FZM-5567, May 15, 1973, General Dynamics, Fort Worth, Texas.

[5] Tennyson, R. C., Chan, K. H., and Muggeridge, D. B., "The Effect of Axisymmetric Shape Imperfections on the Buckling of Laminated Anisotropic Circular Cylinders," *Transactions of the Canadian Aeronautics and Space Institute,* Vol. 4, No. 2, Sept. 1971.

[6] Tennyson, R. C., Muggeridge, D. B., Chan, K. H., and Khot, N. S., *Buckling of Fiber-Reinforced Circular Cylinders Under Axial Compression,* TR-72-102, Aug. 1972. Air Force Flight Dynamics Lab., Wright-Patterson Air Force Base, Ohio.